Engenharia Agrícola

ISSN: 1809-4430 (on-line)

www.engenhariaagricola.org.br

Doi: http://dx.doi.org/10.1590/1809-4430-Eng.Agric.v41n5p536-550/2021

CFD AND TEST OF SINGLE SIDE GANTRY BOOM SPRAYER FOR APPLE ORCHARDS

Peng Huo[1,2], Jianping Li[1*], Pengfei Wang[1], Yongliang Bian[1], Chunlin Xue[1]

[1*]Corresponding author. College of Mechanical and Electrical Engineering, Hebei Agricultural University, Baoding, China. E-mail: ljpnd327@126.com | ORCID ID: https://orcid.org/0000-0003-2807-3888

KEYWORDS

Profiling spray, Computer simulation, Sprayer, RSM, Vertical droplet distribution test.

ABSTRACT

Aiming at addressing the uneven pesticide distribution when spraying high-spindle apple trees, the parameters of a homemade profiling boom sprayer were analysed, and the optimal parameter combinations of the profiling sprayer were determined. Fluent was used to simulate the spray for various parameter values. The goodness of fit (R^2) with experimentally measured data was 0.9270, which verified the accuracy of the numerical simulations. The response surface methodology (RSM) method was used to obtain optimal parameter values from the simulations, and the effective collection rate and spray distribution coefficient of variation were introduced as response values. A sprayer prototype was manufactured based on the optimal parameters determined by RSM analysis, and the results were verified by vertical droplet distribution tests. The results showed that the spray quality increased by 0.7%, 0.9%, and 0.3% for the three best parameters combinations, the droplet distribution was more uniform, and the effect of the profiling spray was better than that of the control tests. The results can provide guidance for the design of sprayers for orchards, and the optimal combination of parameters can provide a basis for subsequent research on precision modelling of profile spraying.

INTRODUCTION

With the continuous development and updating of orchard plant protection machinery, researchers have found that profiling application technology has a good effect on orchard plant protection (Zhai et al., 2018a; Zhou et al., 2017; Liangfu et al., 2018). Various researchers have studied the variable spray required to achieve a profiling spray. For example, Shen et al. 2017 performed plant protection simulation spray tests for an apple orchard based on variations in a single nozzle variable during three different growth stages and found that the spray volume was reduced by 47% to 73%. The ground, tree gap, and air drift loss blindness decreased significantly (Shen et al., 2017). Li et al. 2017a used an automatic profiling sprayer equipped with a laser sensor to detect the volume of the fruit tree canopy and adjust the air volume and spray volume in real time, providing a novel method and innovative equipment for the prevention and control of fruit tree diseases and insect pests (Li et al. 2017b). By studying canopy recognition technology for profile spraying, Hočevar et al., 2010 used an RGB camera and an image recognition machine vision system to implement profile spraying based on the canopy shape, achieving profile and cost reduction (Hočevar et al., 2010). Through an experimental comparison, it was verified that the key parameters, such as the crop height, crop width, crop volume, or leaf area measured by an ultrasonic sensor and lidar sensor, could accurately predict the key canopy parameters. Llorens et al. (2011) achieved a profiling application by studying the adjustment of the nozzle position. Osterman et al. (2013) used laser scanning measurements and a nozzle positioning algorithm to move the nozzle to the optimal spraying position and achieve a profiling spray. The test results showed that the directional profile spraying effectively reduced the drift of the active chemical, the ground deposition, and the required dosage of the active chemical.

Various researchers have studied canopy profiling detection systems to achieve profiling pesticide application (Huiqiang et al., 2007; Gao et al., 2018). Nan et al. (2019) built a plant canopy ultrasonic echo signal detection system based on low-cost ultrasonic sensors and used a cylindrical leaf distribution model to quantify test bench simulations

[1] College of Mechanical and Electrical Engineering, Hebei Agricultural University, Baoding, China
[2] Beijing Key Laboratory of Optimized Design for Modern Agricultural Equipment, China Agricultural University, Beijing, China.

Area Editor: Fábio Lúcio Santos
Received in: 7-6-2021
Accepted in: 8-17-2021

and obtain a quantitative model of the plant canopy density for outdoor fruit tree density measurements. Guien et al. (2004) developed a non-contact profiling-spray position control system with a single-chip microcomputer as the core and achieved profile spraying with a maximum overshoot of 5%. Through the study of automatic target application, Jin et al. (2016) designed an automatic target spraying system, which increased the pesticide utilization rate by 29.7%. Dongmei et al. (2019) used a sprayer equipped with a low-volume profile-spraying orbital test system to test the droplet deposition performance for tea gardens, which improved the adaptability of the low-volume ground profile-spraying technology in tea plant protection operations.

Profiling mechanism adjustment has also been achieved (Zhai et al., 2018b). Kaituo et al. (2019) used a three-degree-of-freedom symmetric two-stage rocker spray mechanism to meet the spray requirements for different fruit tree shapes and realized three-dimensional and efficient profiling pesticide application. Chi et al. (2019) developed a system that could freely switch between vertical spraying mode, 45° inclined spraying mode, and ground spraying mode through a two-way multi-direction automatic spraying device with a loading-mode conversion mechanism. This device met the adaptability requirements of the spraying devices for citrus trees of different sizes.

Air-assisted spraying has the advantages of generating fine droplets with strong penetrability. At present, profile-spraying technology mostly adopts an air-assisted sprayer, and research has mainly focused on variable spraying through the adjustment of the pesticide flow rate of the sprayer and the air flow rate of the fan (Li et al., 2017c). The fixed installation of fans in some orchards may lead to problems related to the application height and the poor adjustability of the application distance. Therefore, to solve problems such as the low application height, the limited application distance, and the poor adaptability for high-spindle fruit trees in an apple orchard, a profile-modelling spray-bar sprayer with an adjustable spraying height and distance must be designed to protect high-spindle apple trees.

In this study, response surface methodology (RSM) was used to optimize the operating parameters of a profile-modelling spray-bar sprayer based on the characteristics of high-spindle apple trees to achieve effective profile-modelling spray.

Sprayer components and operating principle

Sprayer components

A profiling boom sprayer is mainly composed of a chassis, lifting mechanism, folding and unfolding mechanism, spray bar group, pesticide tank, and controller, as depicted in Figure 1. The chassis is the most basic component of the entire device. The chassis carries the lifting mechanism, folding and unfolding mechanism, spray bar group, pesticide tank, and hydraulic station distributor. The lifting mechanism is composed of a slide rail and a hydraulic cylinder. The mechanism is lifted by the hydraulic cylinder. The folding and unfolding mechanism is composed of a double parallel four-bar mechanism, which is driven by a hydraulic cylinder to complete folding and unfolding actions. The spray rod group performs the profiling spraying. As the main working part of the sprayer considered in this study, the fully expanded height of the boom group reached 4.5 m, and the width reached 4 m. Due to the large size of the spray boom and the inconvenient transportation and storage process, the spray boom needs to have a multi-segment design (Xue et al., 2018). The spray boom group was composed of five-section spray booms, which could undergo folding, unfolding, and telescopic actions to complete the fruit tree profiling action.

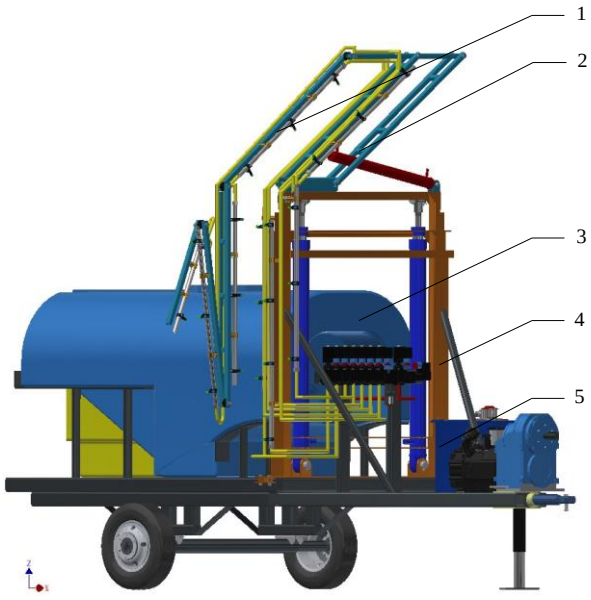

FIGURE 1. Profiling boom sprayer.
1. Spray rod group; 2. Folding and unfolding mechanism; 3. Pesticide tank; 4. Elevator mechanism; 5. Frame

Operating principle

The profiling boom sprayer performed pesticide application in the unfolded state of the spray boom group; it was powered by a tractor. The lifting mechanism and the folding and unfolding structure were controlled by the electric control device. A diaphragm pump was driven by the tractor's power output to transport the liquid pesticide. Controlled by a solenoid valve, the pesticide was sprayed from the nozzles attached to the spray rods at various positions to complete the profiling spray. The spray system is shown in Figure 2.

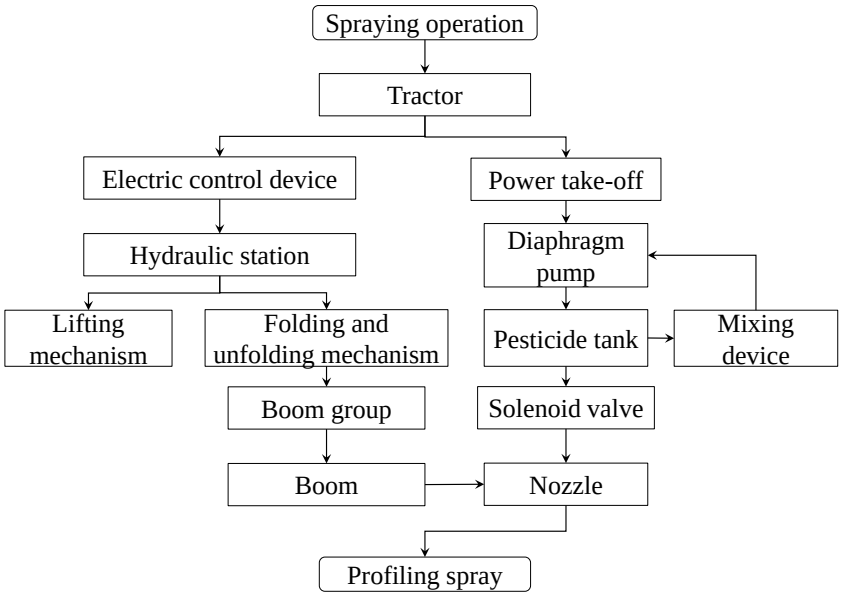

FIGURE 2. Component diagram of the spray system.

Spray operation simulation and benchmarking test

Governing equations

In the simulation of the profiling spray operation, the liquid satisfied the following basic governing equations (Lü et al., 2017).

1) Mass conservation equation:

$$\frac{\partial(\rho u)}{\partial x}+\frac{\partial(\rho v)}{\partial y}+\frac{\partial(\rho w)}{\partial z}=0 \tag{1}$$

Where:

u, v, and w are the velocity components in the x-, y-, and z-directions (m/s), respectively;

t is the time (s), and

ρ is the density (kg/m^3).

2) Momentum equation:

$$\begin{aligned}&\frac{\partial(\rho u)}{\partial t}+div(\rho uU)\\&=-\frac{\partial P}{\partial x}+\frac{\partial \tau_{xx}}{\partial x}+\frac{\partial \tau_{yx}}{\partial y}+\frac{\partial \tau_{zx}}{\partial z}+F_x\\&\frac{\partial(\rho v)}{\partial t}+div(\rho vU)\\&=-\frac{\partial P}{\partial y}+\frac{\partial \tau_{xy}}{\partial x}+\frac{\partial \tau_{yy}}{\partial y}+\frac{\partial \tau_{zy}}{\partial z}+F_y\\&\frac{\partial(\rho w)}{\partial t}+div(\rho wU)\\&=-\frac{\partial P}{\partial z}+\frac{\partial \tau_{xz}}{\partial x}+\frac{\partial \tau_{yz}}{\partial y}+\frac{\partial \tau_{zz}}{\partial z}+F_z\end{aligned} \tag{2}$$

Where:

P is the static pressure (Pa);

τ_{ij} ($i, j = x, y,$ or z) are the components of the viscous stress τ, and

F_x, F_y, and F_z are the volumetric forces in the x-, y-, and z-directions acting on a fluid particle, respectively.

3) Turbulence model

During the spraying operation, the flow velocity at the nozzle exit was high, and the fluid movement was complicated. The turbulence model was used in the simulation. The standard k-ε model, which is a two-equation model (Zhang et al., 2012), was selected because it has the advantages of a high calculation accuracy, simple form, and high versatility. It was assumed that the flow field was completely turbulent, which was convenient for the calculations. The two equations of the k-ε model are as follows.

The turbulent kinetic energy k satisfies the following equation:

$$\begin{aligned}&\frac{\partial(\rho k)}{\partial t}+\frac{\partial(\rho k u_i)}{\partial x_i}\\&=\frac{\partial}{\partial x_j}\left[\left(\mu+\frac{\mu_i}{\sigma_k}\right)\frac{\partial k}{\partial x_j}\right]+G_k+G_b-\rho\varepsilon\end{aligned} \tag{3}$$

And the dissipation rate ε satisfies the following equation:

$$\begin{aligned}&\frac{\partial(\rho\varepsilon)}{\partial t}+\frac{\partial(\rho\varepsilon u_i)}{\partial x_i}=\frac{\partial}{\partial x_j}\left[\left(\mu+\frac{\mu_i}{\sigma_\varepsilon}\right)\frac{\partial \varepsilon}{\partial x_j}\right]\\&+C_{1\varepsilon}\frac{\varepsilon}{k}\left(G_k+C_{3e}G_b\right)+G_b-C_{2\varepsilon}\rho\frac{\varepsilon^2}{k}\end{aligned} \tag{4}$$

Where:

μ_i is the turbulent viscosity coefficient (Pa·s);

k is the turbulent kinetic energy;

G_k is the turbulent kinetic energy generated by the laminar velocity gradient;

G_b is the turbulent kinetic energy generated by buoyancy;

ε is the turbulent dissipation rate of the fluid;

σ_k and σ_ε are the Prandtl numbers corresponding to the turbulent kinetic energy k and the dissipation rate ε, and

$C_{1\varepsilon}$, $C_{2\varepsilon}$, and $C_{3\varepsilon}$ are empirical constants. The following constants were set for the simulations: $C_{1\varepsilon}$ = 1.44, $C_{2\varepsilon}$ = 1.92, $C_{3\varepsilon}$ = 0.09, σ_k = 1.0, and σ_ε = 1.3.

Flow simulations

The spray bar group was equipped with a total of 22 spray heads, 11 on the left and right in the unfolded state, 8 on the vertical rod, and 3 on the oblique rod. The vertical droplet distribution test was benchmarked, so the flow field was simplified as two-dimensional (Jie et al., 2019), and half of the nozzles were selected for the spray operation simulation. The flow field model grid is shown in Figure 3a.

In Fluent, 11 injection points were used to simulate the nozzles. The nozzle spacing and atomization angle could be adjusted by changing the coordinates of the injection points and the x- and y-components of the velocity. The spray parameters were set as follows: the nozzle atomization angle was 60°, the spray distance was 1.25 m, the nozzle spacing was 0.35 m, and the nozzle pressure was 0.6 MPa. The velocity cloud diagram obtained by Fluent is shown in Figure 3b.

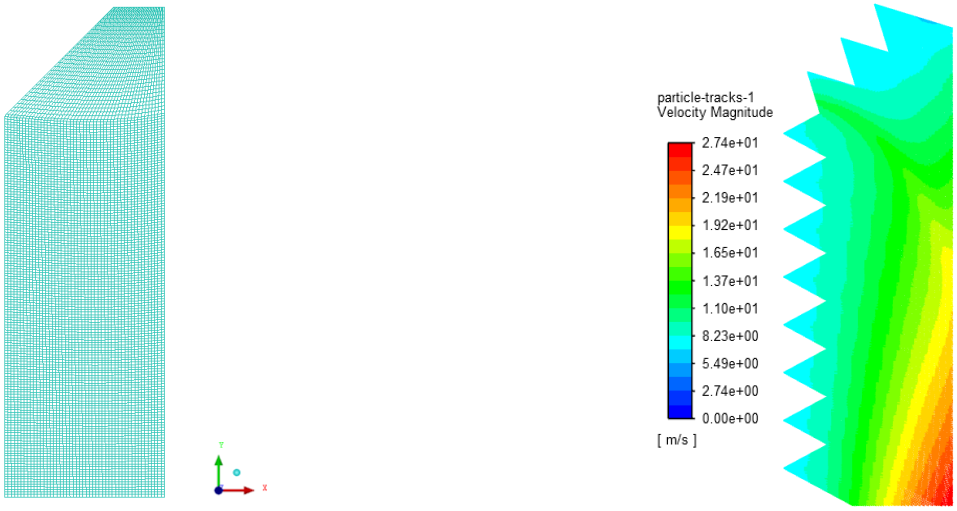

FIGURE 3. Computational fluid dynamics mesh and velocity nephogram. a. Mesh diagram; b. Velocity nephogram.

A new surface was created on the right boundary of the flow field, which was a line in the two-dimensional simulations, and the line was divided into 22.5-cm-long segments from bottom to top to collect the spray droplets, as shown in Figure 4a. A total of 20 collection units were used as droplet collectors, named Ma, ab, bc, cd, ... , qr, rs, st, as shown in Figure 4a. Each collection unit was numbered from 1 to 20 from bottom to top, and the droplet deposition amount (mass flow) of each collection unit was derived. The result is shown in Figure 4b.

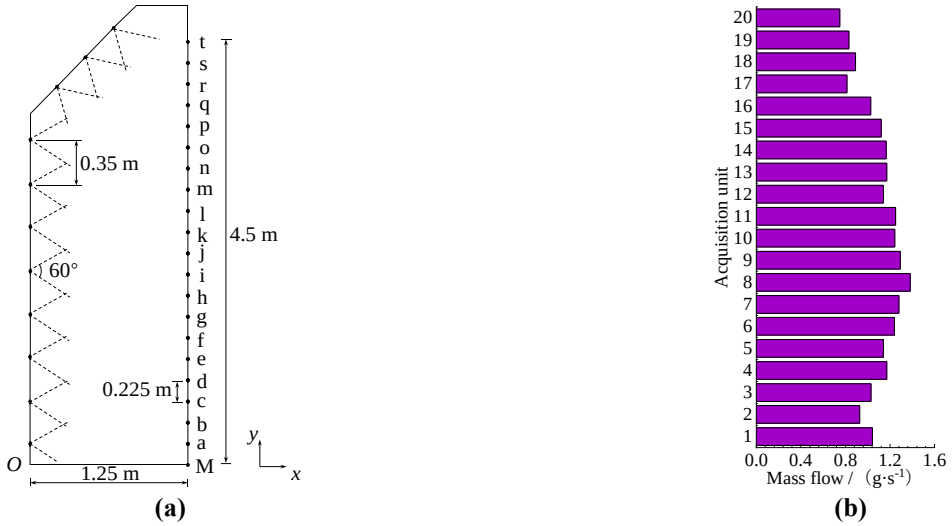

FIGURE 4. Schematic diagram of the mass flow acquisition unit and mass flow in each interval.
(a) Acquisition unit; (b) Mass flow.

Benchmarking test and model verification

Trial prototypes with the structural parameters of the simulation model were used to verify the accuracy of the simulation results (Qu et al., 2017). The test was carried out on August 28, 2020, at the test site of Baozhong Agricultural Tools Factory, Gaobeidian City, Hebei, China. The work site is shown in Figure 5. The test environment had an average temperature of 35.4 °C, an average humidity of 35%, and a natural wind speed of 1.23 $m \cdot s^{-1}$.

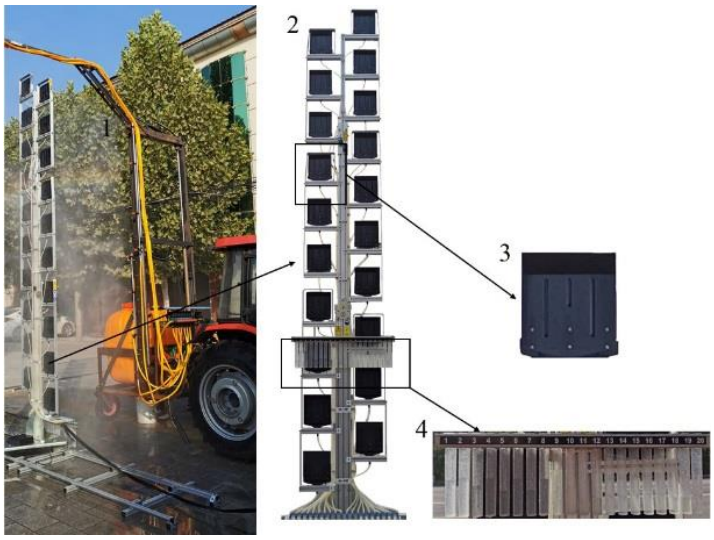

FIGURE 5. Calibration test site.
1. Profiling boom sprayer; 2. Vertical droplet distribution measuring instrument; 3. Droplet collection unit; 4. Layered measuring instrument.

The profiling boom sprayer and the tractor (Dongfanghong MF454) were relatively stationary, and the vertical droplet distribution measuring instrument (ARTS904520, Italy AAMS company) slid to achieve a relative motion form. The test was repeated three times at a forward speed of 0.1 $m \cdot s^{-1}$. The three tests were named Group 1, Group 2, and Group 3, and each test was carried out for 30 s. To prevent the residual droplets on the collection unit of the vertical droplet distribution measuring instrument from affecting the results, the interval between each test was 30 min, and the test was repeated after the droplets were completely deposited (Zhou et al., 2016).

The liquid used in the benchmark test was distilled water, and the density of the distilled water was approximately 1 $g \cdot ml^{-1}$, so the droplet deposition volume (ml) was replaced by the droplet deposition mass (g). The amount of spray during the 30 s test time (g) was expressed in the form of a droplet mass flow rate ($g \cdot s^{-1}$), and the three test results are summarized in Table 1.

TABLE 1. Droplet deposition in the three groups.

Acquisition unit	Amount of mist deposition/($g \cdot s^{-1}$)				
	Group 1	Group 2	Group 3	Mean	Simulation
1	0.630	0.790	0.662	0.694	0.812
2	0.907	1.064	0.996	0.989	1.041
3	0.769	0.927	0.830	0.842	0.927
4	1.285	1.051	0.980	1.105	1.030
5	1.066	1.220	1.187	1.158	1.171
6	1.478	1.183	1.141	1.267	1.140
7	1.150	1.302	1.287	1.246	1.240
8	1.984	1.350	1.345	1.560	1.280
9	1.514	1.622	1.493	1.543	1.381
10	1.391	1.179	1.364	1.312	1.293
11	1.323	1.473	1.293	1.363	1.244
12	1.331	1.481	1.301	1.371	1.250
13	1.313	1.330	1.141	1.261	1.140
14	1.221	1.373	1.186	1.260	1.171
15	1.398	1.365	1.177	1.313	1.165
16	1.263	1.306	1.138	1.236	1.122
17	1.022	1.177	1.198	1.132	1.028
18	0.830	1.045	0.776	0.883	0.890
19	0.746	0.905	0.688	0.780	0.830
20	0.634	0.795	0.611	0.680	0.750

To verify the reliability of the model, a linear fit of the simulated droplet flow rates and the average droplet flow rates of the three tests was performed, and the result is shown in Figure 6. The fitted equation was as follows:

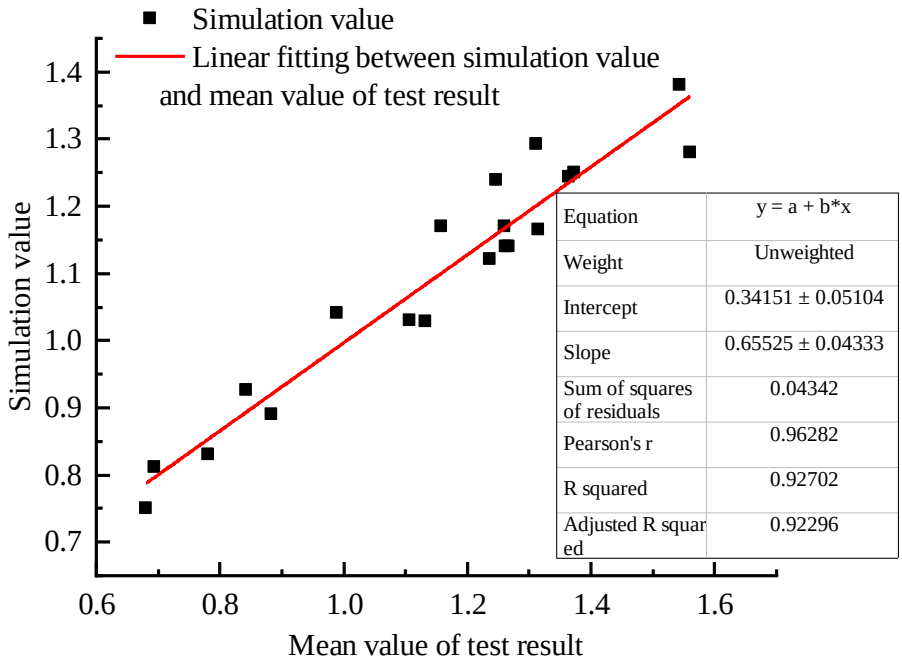

FIGURE 6. Linear fit between simulated and measured values of the droplet flow rate.

$$y = 0.6552x + 0.3416 \quad (5)$$

The goodness of fit R^2 was 0.9270, indicating that the simulated values were linearly related to the experimental values (Ding et al., 2016). This result showed that the established model and calculation method were reasonable, and the subsequent simulation results based on this model were reliable.

Optimization analysis

Response surface methodology (RSM)

Optimization scheme design

Fluent was used to determine the droplet deposition (mass flow) in each collection unit. The structural parameters and spray conditions were divided into three groups corresponding to spray atomization angles of 60°, 80°, and 110° for subsequent optimization analysis. The effective collection rate was introduced as the evaluation index of the droplet deposition in this study (Zhichong et al., 2020), defined as follows:

$$\text{Effective collection rate} = \frac{\text{Droplet mass flow}}{\text{Total displacement}} \times 100\% \quad (6)$$

The total displacement was 30 g·s^{-1}. In addition, the coefficient of variation of the droplet distribution was introduced as an evaluation index of the uniformity of the droplet distribution (Yang et al., 2015), defined as follows:

$$\text{Coefficient of variation} = \frac{\text{Standard deviation of droplet deposition}}{\text{Average droplet deposition}} \times 100\% \quad (7)$$

The nozzle pressure, spray distance, and nozzle spacing were selected as factors, and the effective collection rate and coefficient of variation were selected as responses for the RSM optimization analysis (Cheng et al., 2017a). The factor levels and codes are shown in Table 2.

TABLE 2. Factor levels of response surface optimization analysis.

Level	Factor		
	Nozzle pressure *A*/MPa	Spray distance *B*/m	Nozzle distance *C*/m
1	0.8	1.5	0.4
0	0.7	1.25	0.35
-1	0.6	1	0.3

Orthogonal experimental design tables were generated using the Design-Expert software central composite design (central composite design, abbreviated as CCD) (Cheng et al., 2017b). As an example, the test design scheme and response values for a 60° spray angle are shown in Table 3.

TABLE 3. Test design scheme and response value for a 60° atomization angle.

Group	Nozzle pressure A/MPa	Spray distance B/m	Nozzle distance C/m	Effective collection rate Y_{60}/%	Coefficient of variation $C.V_{60}$/%
1	0	−1	0	73.15	17.24
2	0	0	0	73.72	17.04
3	1	1	−1	70.97	18.45
4	−1	0	0	71.16	17.18
5	−1	1	1	70.09	18.98
6	0	0	0	73.68	17.03
7	1	0	0	72.05	17.18
8	0	0	0	73.69	17.02
9	0	1	0	72.95	17.45
10	0	0	1	73.14	17.95
11	1	−1	1	72.78	18.16
12	−1	−1	−1	73.13	18.58
13	0	0	−1	73.05	18.07

Establishment and analysis of regression model

The combination of the operating conditions and parameters was further optimized. In this section, the effective collection rate is denoted as Y_{60}, the coefficient of variation is denoted as $C.V_{60}$, the factor nozzle pressure is denoted as A, the spray distance is denoted as B, and the nozzle spacing is denoted as C. The significance of the regression model and the analysis of variance results are shown in Table 4.

TABLE 4. Regression Model p value and significance for the 60° atomization angle.

Source of variance	p value	p value	Significance
Model	< 0.0001	< 0.0001	Significant
A	0.0009	1.0000	
B	0.0596	0.0082	
C	0.2751	0.0371	
AB	0.0895	0.0235	
AC	0.0450	0.0459	
BC	0.2281	0.0014	
A^2	< 0.0001	0.0013	
B^2	0.0003	0.0002	
C^2	0.0004	< 0.0001	
Lack of fit	0.0654	0.0615	Not significant

The overall p values of the Y_{60} model and the $C.V_{60}$ model were both less than 0.01, which indicated that the models were extremely significant. The p values of the lack-of-fit term were both greater than 0.05 and thus were not significant. The adjusted coefficient of determination R^2_{Adj} values were both 0.9988, indicating that the model fitting effect was good and that the models could be used to analyse and predict the response values (Yuan et al., 2012). The coefficient of the first-order term, A, of the Y_{60} model was extremely significant, while B and C were not significant. For the interaction terms, AC was significant, while AB and BC were not. For the second-order terms, A^2, B^2, and C^2 were extremely significant. The following regression equation was established:

$$\begin{aligned} Y_{60} = & -72.04 + 294.59 \times A + 18.79 \times B + 167.98 \times C \\ & + 4.10 \times AB - 27.50 \times AC + 5.00 \times BC \\ & - 204.03 \times A^2 - 9.52 \times B^2 - 220.11 \times C^2 \end{aligned} \quad (8)$$

Figure 7 shows the response surfaces of the effective collection rate of the droplets as functions of the nozzle pressure, spray distance, and nozzle spacing when the atomization angle was 60°. The effects of the nozzle pressure, spray distance, and nozzle spacing can be readily distinguished from these surfaces.

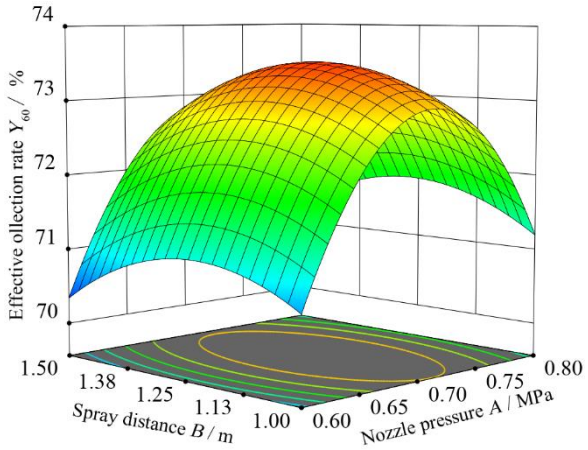

(a)

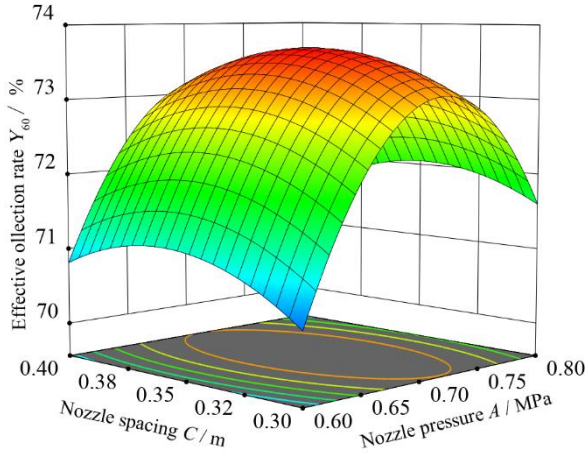

(b)

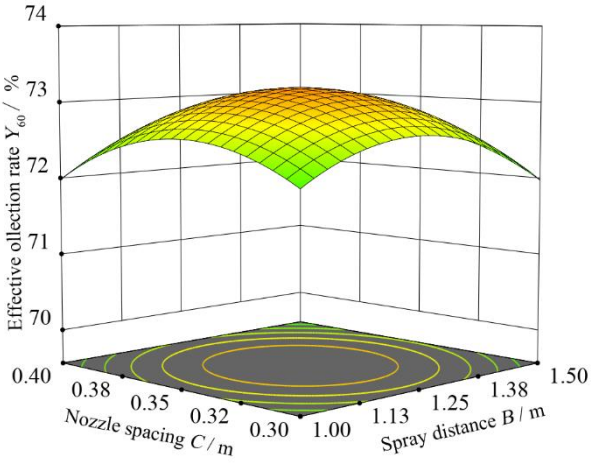

(c)

FIGURE 7. Response surface of the droplet effective collection rate for a 60° spray angle.
(a) Nozzle pressure and spray distance; (b) Nozzle pressure and nozzle spacing; (c) Spray distance and nozzle spacing.

The coefficient of the first-order term, B, of the $C.V_{60}$ model was extremely significant, C was significant, and A was not significant. For the interaction terms, BC was extremely significant, and AB and AC were significant. For the second-order terms, A^2, B^2, and C^2 were extremely significant. The fitted regression equation was as follows:

$$\begin{aligned} C.V_{60} = {} & 85.24 - 15.48 \times A - 17.40 \times B - 297.05 \times C \\ & -3.50 \times AB - 13.50 \times AC + 19.00 \times BC \\ & +17.55 \times A^2 + 5.45 \times B^2 + 402.22 \times C^2 \end{aligned} \quad (9)$$

Figure 8 shows the surfaces of the coefficient of variation of the droplet distribution as functions of the nozzle pressure, spray distance, and nozzle spacing when the atomization angle was 60°.

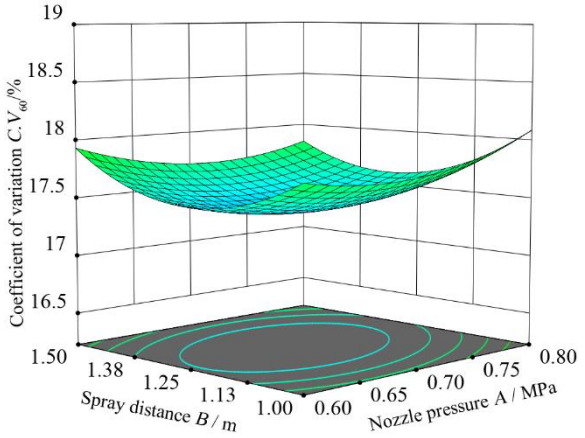

(a)

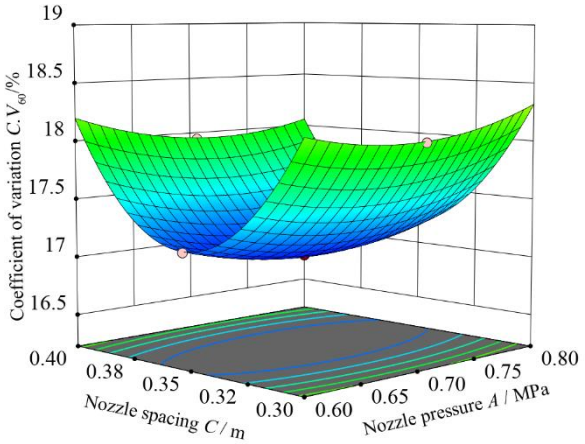

(b)

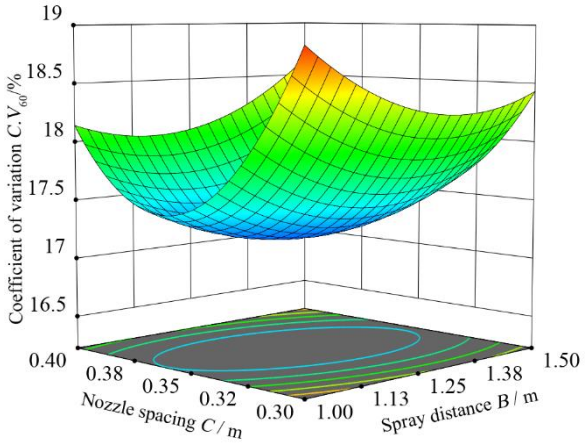

(c)

FIGURE 8. Response surface of the droplet distribution variation coefficient for a 60° spray angle.
(a) Nozzle pressure and spray distance; (b) Nozzle pressure and nozzle spacing; (c) Spray distance and nozzle spacing.

Similarly, the regression equations for the spray nozzle atomization angles of 80° and 110° were established as follows:

spray angle of 80°:

$$\begin{aligned} Y_{80} = & -5.86 + 125.35 \times A + 17.76 \times B + 153.30 \times C \\ & + 9.40 \times AB + 38.00 \times AC + 22.00 \times BC \\ & - 107.61 \times A^2 - 12.98 \times B^2 - 298.43 \times C^2 \end{aligned} \quad (10)$$

$$C.V_{80} = 80.80 - 62.37 \times A - 25.93 \times B - 139.34 \times C + 2.50 \times AB - 68.50 \times AC - 12.60 \times BC + 59.01 \times A^2 + 11.12 \times B^2 + 288.05 \times C^2 \quad (11)$$

spray angle of 110°:

$$Y_{110} = -104.28 + 200.12 \times A + 67.89 \times B + 383.34 \times C - 26.70 \times AB + 75.50 \times AC - 12.20 \times BC - 136.61 \times A^2 - 17.92 \times B^2 - 614.05 \times C^2 \quad (12)$$

$$C.V_{110} = 103.06 - 83.65 \times A - 54.77 \times B - 136.11 \times C - 3.10 \times AB - 10.50 \times AC + 37.40 \times BC + 67.32 \times A^2 + 17.73 \times B^2 + 139.29 \times C^2 \quad (13)$$

RESULTS AND DISCUSSION

As mentioned above, Y and $C.V$ are important evaluation indices for droplet deposition. They were used as optimization targets in the optimization model. It is expected that Y will be maximized as $C.V$ is minimized. Thus, the spray quality is defined as follows: $f = Y - C.V$. The optimization problem with the constraints of the nozzle pressure A, the calculated spray distance B, and the nozzle distance C is expressed as follows:

$$\begin{cases} \max: f = Y - C.V \\ s.t. \begin{cases} 0.60 \le A \le 0.80 \\ 1.00 \le B \le 1.50 \\ 0.30 \le C \le 0.40 \end{cases} \end{cases} \quad (14)$$

For nozzle atomization angles of 60°, 80°, and 110°, the objective functions (f_{60}, f_{80}, and f_{110}) were optimized under the constraint conditions to obtain the optimal value of each parameter. At the same time, to test the reliability of the optimization results, the optimal parameters were input into the model and three repeated simulations were conducted. The results are listed in Table 5.

TABLE 5. RSM optimization results and verification.

Spray angle of nozzle/°	Optimization results			Effective collection rate Y/%	Coefficient variations $C.V$/%	Spray quality f/%	Mass flow /(g·s^{-1})	Mean value of repeated simulation results /(g·s^{-1})	Relative error/%
	Nozzle pressure A/MPa	Spray distance B/m	Nozzle distance C/m						
60	0.71	1.23	0.35	73.71	17.01	56.69	22.113	21.295	3.69
80	0.70	1.26	0.35	75.32	17.42	57.91	22.596	21.073	6.74
110	0.69	1.25	0.34	74.53	17.21	57.32	22.359	21.359	4.25

The relative errors between the optimization and simulation results in the three cases were less than 10%, and thus, the regression model could suitably predict the simulation results (Changling et al., 2020). The optimal results from the RSM optimization are expressed in the form of "nozzle atomization angle–nozzle pressure–spray distance–nozzle spacing." The optimal combinations were 60–0.71–1.23–0.35, 80–0.70–1.26–0.35, and 110–0.69–1.25–0.34 and were named Part1, Part2, and Part3, respectively. The coefficient of variation of the Part2 group was relatively high, indicating that the droplet distribution of this group was relatively uniform. To verify the uniformity of the droplet distribution and the spray quality of the optimal parameter combination, subsequent field test verification was performed.

Field test

Tree survey

A survey was conducted in a densely planted apple orchard on Danfeng Mountain (38°N, 115°E), Tang County, Baoding City, Hebei Province. High-spindle-shaped trees have also been referred to as cylindrical (Ma et al., 2014). The top, middle, and bottom parts of the canopy were crowned. The tree widths were 0.8–1.2 m, the heights were 3.5–4.0 m, and the total number of side branches on the main trunks was 20–30. Figure 9 shows a photograph and schematic representation of a high-spindle-shaped apple tree. Therefore, when planting high-spindle apple trees, to achieve the goal of profiling pesticide application, it is necessary to deliver a uniform droplet distribution in the upper, middle, and lower canopies.

FIGURE 9. High fusiform apple orchard and high-fusiform diagram.
1. High-fusiform apple orchard; 2. High-fusiform tree diagram.

FIELD TEST, RESULTS AND DISCUSSION

Based on the three sets of optimal parameters obtained from the optimization analysis of the simulations, a prototype was developed, and the sprayer application effect was studied through field tests. Tests for each group of spray parameters were repeated three times, and tests with three groups of control group CK parameter combinations, 60–0.75–1.25–0.35, 80–0.75–1.25–0.35, and 110–0.75–1.25–0.35, were conducted for comparison. The test process was as described above. The volumes of droplets collected in the collection test tubes during the tests were recorded, and the results are shown in Figure 10.

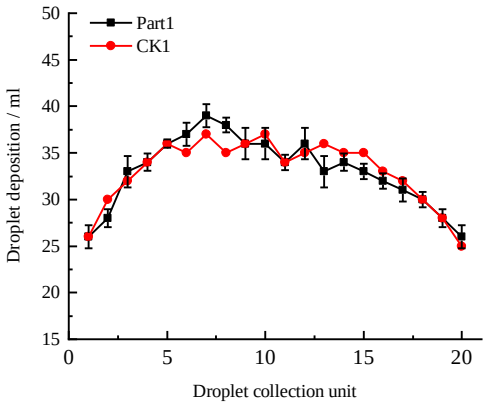

(a)

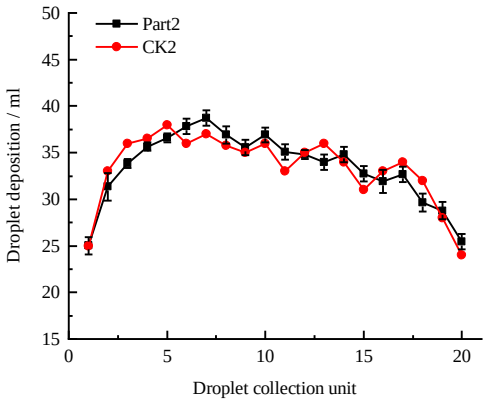

(b)

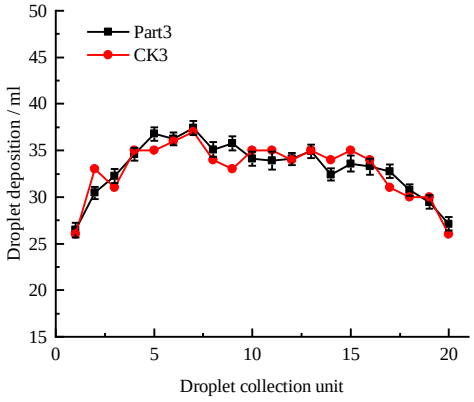

(c)

FIGURE 10. Droplet deposition for three optimal combinations of parameters.
(a) Droplet deposition of Part1 and CK1; (b) Droplet deposition of Part2 and CK2; (c) Droplet deposition of Part3 and CK3.

The three groups of test results were analysed and compared with the control group, as shown in Figure 11. The results showed that the spray quality was increased by 0.7%, 0.9%, and 0.3% for Part1, Part2 and Part3, respectively.

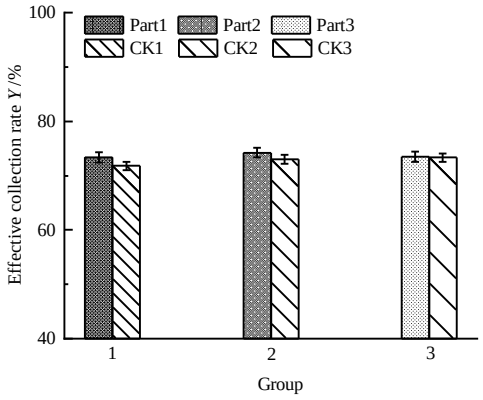

(a)

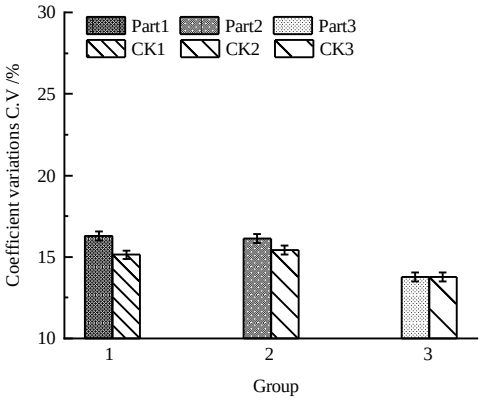

(b)

FIGURE 11. Spray quality performance index for the control and optimal parameter groups.
(a) Droplet effective collection rate; (b) Droplet distribution coefficient of variation.

Based on the above analysis, for the optimized three sets of spray parameters (60–0.71–1.23–0.35, 80–0.70–1.26–0.35, and 110–0.69–1.25–0.34), the spray quality of the prototype was better than that of the control group, and the droplet distributions were more uniform. This indicated that the profiling effect was better.

CONCLUSIONS

Based on the design goal of the profiling spray, the operating conditions and parameters of an orchard boom sprayer were optimized and tested, and the following conclusions were obtained:

1) The goodness of fit R^2 between the numerical simulation results and the benchmark test results was 0.9270, and thus, the simulation model was reliable.

2) The RSM optimization yielded three sets of operating parameters with the best effective droplet collection rate. The optimal combinations of nozzle atomization angle–nozzle pressure–spray distance–nozzle spacing were 60–0.71–1.23–0.35, 80–0.70–1.26–0.35, and 110–0.69–1.25–0.34.

3) Three sets of parameter combinations with improved profiling effects were obtained. The optimization results were verified by field tests and compared with the control group, and the spray quality in the optimized parameter tests increased by 0.7%, 0.9%, and 0.3% for the 60–0.71–1.23–0.35, 80–0.70–1.26–0.35, and 110–0.69–1.25–0.34 parameter combinations, respectively, indicating that the droplet distributions were more uniform and that the profiling effect was better. These results can be used for the profiling application of high-spindle fruit trees.

In the future, it will be necessary to obtain data through field experiments to comprehensively consider the combination of operating conditions and parameters to achieve a uniform droplet distribution and droplet penetration, explore the design concepts of orchard profiling sprayers, and apply pesticides for sprayers in orchards. The selection of parameters obtained in this paper can serve as a reference for spraying operations.

ACKNOWLEDGEMENTS

We thank LetPub (www.letpub.com) for linguistic assistance and pre-submission expert review. This work is supported by the earmarked fund for Agriculture Research System of China (CARS-27), the earmarked fund for Hebei Fruit Innovation Team of Modern Agro-industry Technology Research System (HBCT2018100205).

REFERENCES

Changling W, Xiongkui H, Aijun Z (2020) Measuring method and experiment on spray drift of chemicals applied by UAV sprayer based on an artificial orchard test bench. Transactions of the Chinese Society of Agricultural Engineering 36(13): 56-66.

Cheng Z, Qi L, Wu Y, Cheng Y, Yang Z, Gao C (2017a) Parameter optimization on swing variable sprayer of orchard based on RSM. Transactions of the Chinese Society for Agricultural Machinery 48(S1): 22-29.

Chi M, Guanglin L, Xiaodong L (2019) Development of multi-orientation automatic spraying device for citrus orchards in hilly and mountainous areas. Transactions of the Chinese Society of Agricultural Engineering (Transactions of the CSAE), 35(3): 31-41.

Ding T, Cao S, Xue X, Ding S, Zhou L, Qiao B (2016) Simulation and experiment on single-channel and double-channel airflow field of orchard sprayer. Transactions of the Chinese Society of Agricultural Engineering 32(14): 62-68.

Dongmei L, Hangxu Y, Hongping Z, Yu R, Jiaqiang Z, Yulong N (2019) Droplet deposition performance of low-capacity profiling spray in densely planted dwarf tea plantation. Transactions of the Chinese Society for Agricultural Machinery 50(10): 96-105.

Gao G, Xiao K, Li J (2018) Precision Spraying Model Based on Kinect Sensor for Orchard Applications. Applied Engineering in Agriculture 34(2): 291-298.

Guien W, Tiansheng H, Jie L, Xinrong K, Xuejun Y (2004) Position control system of profile modeling spray for fruit trees. Transactions of The Chinese Society of Agricultural Engineering (3): 81-84.

Hočevar M, Širok B, Jejčič V, Godeša T, Lešnika M, Stajnko D (2010) Design and testing of an automated system for targeted spraying in orchards. Journal of Plant Diseases and Protection 117(2): 71-79.

Huiqiang L, Caixing L, Tiansheng H, Lei X, Wenmeng G. (2007) Neural network mixed model for profile modeling spray of fruit trees based on GA. Transactions of the Chinese Society of Agricultural Engineering 23(10): 167-171.

Jie L, Chunqing Z, Shanjun L (2019) Droplet deposition characteristics of CFD based orchard air-driven sprayer. Journal of Huazhong Agricultural University 38(06): 171-177.

Jin X, Dong X, Yang XJ (2016) Design and experiment of target spraying system of 3WGZ-500 sprayer. Trans Chinese Soc Agric Mach 47(7): 21-27.

Kaituo F, Hailang G, Yunyang S (2019) Optimization and simulation of profile spraying mechanism based on ADAMS. Journal of Chinese Agricultural Mechanization 40(10): 58-63.

Li L, He X, Song J, Liu Y, Wang Z, Li J, Liu Z (2017a) Comparative experiment on profile variable rate spray and conventional air assisted spray in orchards. Transactions of the Chinese Society of Agricultural Engineering 33(16): 56-63.

Li L, He X, Song J, Wang X, Jia X, Liu C (2017b) Design and experiment of automatic profiling orchard sprayer based on variable air volume and flow rate. Transactions of the Chinese Society of Agricultural Engineering 33(1): 70-76.

Liangfu Z, Ling Z, Xinyu X, Chen C (2018) Research progress and application status of electrostatic pesticide spray technology. Transactions of the Chinese Society of Agricultural Engineering (Transactions of the CSAE), 34(18): 1-11.

Llorens J, Gil E, Llop J (2011) Ultrasonic and LIDAR sensors for electronic canopy characterization in vineyards: Advances to improve pesticide application methods. Sensors 11(2): 2177-2194.

Lü X, Zhang M, Chang Y, Lei X, Yang Q (2017) Influence of deflector angles for orchard air-assisted sprayer on 3D airflow distribution. Transactions of the Chinese Society of Agricultural Engineering 33(15): 81-87.

Ma X, Meng Q, Zhang L, Liu G, Zhou W (2014) Image mosaics reconstruction of canopy organ morphology of apple trees. Transactions of the Chinese Society of Agricultural Engineering 30(12): 154-162.

Nan Y, Zhang H, Zheng J, Jiao X, Xu Y, Wang G (2019) Ultrasonic quantification test of plant canopy density based on cylindrical surface model. Transactions of the Chinese Society for Agricultural Machinery 50(1): 209-216.

Osterman A, Godeša T, Hočevar M, Širok B, Stopar M (2013) Real-time positioning algorithm for variable-geometry air-assisted orchard sprayer. Computers and electronics in agriculture 98: 175-182.

Qu F, Sheng X, Li X, Zhang J, Li W, Liu J (2017) Improved design of 3WZF-400A orchard air-assisted sprayer. Transactions of the Chinese Society for Agricultural Machinery 48(S1): 15-21.

Shen Y, Zhu H, Liu H, Chen Y, Ozkan E (2017) Development of a laser-guided, embedded-computer-controlled, air-assisted precision sprayer. Transactions of the ASABE 60(6): 1827-1838.

Xue T, Li W, Du YF, Mao ER, Wen HJ (2018) Adaptive fuzzy sliding mode control of spray boom active suspension for large high-clearance sprayer. Transactions of the CSAE 34(21): 47-56.

Yang Z, Niu M, Li J, Xu X, Xu J, Chen Z (2015) Design and experiment of an electrostatic sprayer with online mixing system for orchard. Transactions of the Chinese Society of Agricultural Engineering 31(21): 60-67.

Yuan X, Qi L, Wang H, Huang S, Ji R, Zhang J (2012) Spraying parameters optimization of swing, automatic variables and greenhouse mist sprayer with response surface method. Transactions of the Chinese Society for Agricultural Machinery 43(4): 45-54.

Zhai C, Xu S, Long J, Li H, Zhang B, Zhu R (2018a) Optimization design of orchard air-assisted sprayer and mathematical model for spray height control. Journal of Northwest A & F University-Natural Science Edition 46(9): 148-154.

Zhai C, Zhao C, Ning W, Long J, Wang X, Weckler P, Zhang H (2018b) Research progress on precision control methods of air-assisted spraying in orchards. Transactions of the Chinese Society of Agricultural Engineering 34(10): 1-15.

Zhang T, Yang X, Yan H, Wang J, Dong X (2012) Anti-drift technology of super-high clearance boom sprayer with air-assisted system. Transactions of the Chinese Society for Agricultural Machinery 43(12): 77-86.

Zhichong W, Herbst A, Bonds J (2020) Stereoscopic test method for low-altitude and low-volume spraying deposition and drift distribution of plant protection UAV. Transactions of the Chinese Society of Agricultural Engineering 36(04): 54-62.

Zhou L, Xue X, Zhou L, Zhang L, Ding S, Chang C, Chen C (2017) Research situation and progress analysis on orchard variable rate spraying technology. Transactions of the Chinese Society of Agricultural Engineering 33(23): 80-92.

Zhou L, Zhang L, Xue X, Ding W, Sun Z, Zhou Q, Cui L (2016) Design and experiment of 3WQ-400 double air-assisted electrostatic orchard sprayer. Transactions of the Chinese Society of Agricultural Engineering 32(16): 45-53.